Brown adipose tissue whitening leads to brown adipocyte death and adipose tissue inflammation[S]

Petra Kotzbeck,[1,2,3,]* Antonio Giordano,[1,†] Eleonora Mondini,[†] Incoronata Murano,[†] Ilenia Severi,[†] Wiebe Venema,[†] Maria Paola Cecchini,[§] Erin E. Kershaw,** Giorgio Barbatelli,[†] Guenter Haemmerle,* Rudolf Zechner,*[,††] and Saverio Cinti[3,†]

Institute of Molecular Biosciences,* University of Graz, Graz, Austria; Department of Experimental and Clinical Medicine and Center of Obesity,[†] University of Ancona (Politecnica delle Marche)-United Hospitals, Ancona, Italy; Department of Neurosciences, Biomedicine, and Movement Sciences,[§] University of Verona, Verona, Italy; Division of Endocrinology and Metabolism,** Department of Medicine, University of Pittsburgh, Pittsburgh, PA; and BioTechMed-Graz,[††] Graz, Austria

Abstract In mammals, white adipose tissue (WAT) stores and releases lipids, whereas brown adipose tissue (BAT) oxidizes lipids to fuel thermogenesis. In obese individuals, WAT undergoes profound changes; it expands, becomes dysfunctional, and develops a low-grade inflammatory state. Importantly, BAT content and activity decline in obese subjects, mainly as a result of the conversion of brown adipocytes to white-like unilocular cells. Here, we show that BAT "whitening" is induced by multiple factors, including high ambient temperature, leptin receptor deficiency, β-adrenergic signaling impairment, and lipase deficiency, each of which is capable of inducing macrophage infiltration, brown adipocyte death, and crown-like structure (CLS) formation. Brown-to-white conversion and increased CLS formation were most marked in BAT from adipose triglyceride lipase (*Atgl*)-deficient mice, where, according to transmission electron microscopy, whitened brown adipocytes contained enlarged endoplasmic reticulum, cholesterol crystals, and some degenerating mitochondria, and were surrounded by an increased number of collagen fibrils. Gene expression analysis showed that BAT whitening in *Atgl*-deficient mice was associated to a strong inflammatory response and NLRP3 inflammasome activation.■ Altogether, the present findings suggest that converted enlarged brown adipocytes are highly prone to death, which, by promoting inflammation in whitened BAT, may contribute to the typical inflammatory state seen in obesity.—Kotzbeck, P., A. Giordano, E. Mondini, I. Murano, I. Severi, W. Venema, M. P. Cecchini, E. E. Kershaw, G. Barbatelli, G. Haemmerle, R. Zechner, and S. Cinti. **Brown adipose tissue whitening leads to brown adipocyte death and adipose tissue inflammation.** *J. Lipid Res.* 2018. 59: 784–794.

Supplementary key words brown fat • white adipose tissue • white adipocyte • adipose triglyceride lipase • adipocyte size • macrophage • nucleotide-binding oligomerization domain-like receptor-3 inflammasome

Obesity is a major and growing public health problem. Reports based on the BMI (weight/height^2), an indirect marker of adiposity, have shown that over the past decades, obesity has been increasing worldwide (1). Obesity is a severe clinical problem, because it is associated with an increased risk of developing a variety of medical conditions, such as insulin resistance, hypertension, dyslipidemia, nonalcoholic fatty liver, cardiovascular disease, and even some cancers. Importantly, it is the major risk factor for type 2 diabetes (2, 3).

Adipose tissue dysfunction and inflammation are hallmarks of morbid obesity. In obese mice and humans, adipose tissue is infiltrated by inflammatory cells and produces inflammatory mediators that link fat accumulation to cardiovascular and metabolic complications, such as insulin resistance and type 2 diabetes (4–9). Macrophages are the main inflammatory cells found in inflamed adipose tissue. Here, monocyte-derived macrophages positive for MAC-2 often localize around dead adipocytes and form the so-called crown-like structures (CLSs) (6), where aggregates of activated macrophages, sometimes fused into syncytia (multinucleated giant cells), surround and clear dead

adipocytes. Importantly, macrophage infiltration of obese fat positively correlates with adipocyte size and CLS density (4–7). In particular, the number of CLSs in obese fat is in direct proportion to the degree of adipocyte hypertrophy in both visceral and subcutaneous adipose tissue (7). However, their density is higher in visceral adipose tissue, where adipocytes are smaller, than in subcutaneous fat, where adipocytes are larger. This suggests that lipid overload results in adipocyte growth up to a critical size; growth beyond this size induces profound cell stress and leads to death. Thus, the critical size is smaller in visceral than in subcutaneous fat depots (6, 7). Hypertrophic adipocytes from obese mice are prone to developing organelle dysfunction, such as endoplasmic reticulum (ER) stress (10), mitochondrial dysfunction (11), and activation of the NLRP3 inflammasome pathway, suggesting that hypertrophic stressed adipocytes undergo pyroptotic cell death and initiate an inflammatory response (12). Notably, organelle dysfunction and inflammasome activation are more marked in visceral than in subcutaneous adipocytes (12).

The mammalian adipose organ contains white and brown adipocytes (13). White adipocytes, which are found in white adipose tissue (WAT), store dietary energy as triglycerides in a single large lipid droplet (unilocular adipocytes); at times of high calorie requirements, triglycerides undergo hydrolyzation and the resulting fatty acids are secreted into the bloodstream and supplied to other tissues. Brown adipocytes are the main parenchymal cell type found in brown adipose tissue (BAT). They are characterized by multiple small triglyceride droplets (multilocular adipocytes) and contain numerous large mitochondria, where uncoupling protein 1 (UCP1) enables use of the energy derived from fatty acid oxidation for heat generation (nonshivering thermogenesis) (14). In normally fed mice maintained at normal ambient temperature, white and brown adipocytes are found together in several subcutaneous and visceral depots (13–16). In contrast, in the adipose organ of obese animals and humans, typical brown adipocytes are barely detectable because most of them undergo a still poorly elucidated conversion to a "white-like" phenotype (13, 17, 18). Given the limited available data on the fate and possible proinflammatory role of white-like adipocytes derived from brown-to-white conversion in obese mice, the present study was performed to investigate the implications of brown-to-white-like conversion (in terms of the tendency of adipocytes to develop inflammation and to die) in the adipose depots of mice challenged with environmental, dietary, and genetic stimuli.

MATERIAL AND METHODS

Animals and tissues

Adipose triglyceride lipase (*Atgl*)-knockout (ko) mice generated by targeted homologous recombination (19) were backcrossed at least seven times to a C57BL/6J genetic background. All experiments were carried out in male 8- to 10-week-old *Atgl*-ko mice and corresponding wild-type littermates. The adipose-specific *Atgl*-ko (AAKO) mice (20) are described in the supplemental

Materials and Methods. *Db/+* and *db/db* female mice aged 5 weeks were purchased from Charles River (Lecco, Italy) and used for experimental procedures at 14 weeks of age (five animals per strain). C57BL/6J female mice (Harlan, Udine, Italy) aged 12 weeks were kept at 28°C (n = 5, warm-acclimated mice) or at 6°C (n = 5, cold-acclimated mice) for 10 days to reduce and respectively increase the noradrenergic inputs to the adipose organ. Adult mice lacking β-adrenergic receptors (β-less mice) were kindly provided by Dr. B. B. Lowell (Harvard Medical School, Boston, MA) (21). Animals were individually caged and maintained on a 12:12 h light/dark cycle with free access to standard pellet food and water. The animal experiments performed at the Department of Experimental and Clinical Medicine, Università Politecnica delle Marche, Ancona, Italy were in accordance with institutional and national guidelines and were approved by the institutional Animal Ethics Board of Università Politecnica delle Marche. Experiments carried out at the Institute of Molecular Biosciences, University of Graz, Graz, Austria were approved and performed according to the guidelines of the ethics committee of the University of Graz and the Austrian Federal Ministry for Science and Research.

For morphological studies, mice were euthanized with an overdose of anesthetic (Avertin; Fluka Chemie, Buchs, Switzerland) and immediately perfused with 4% paraformaldehyde in 0.1 M phosphate buffer (PB), pH 7.4, for 5 min. BAT and WAT depots were dissected using a Zeiss OPI1 surgical microscope (Carl Zeiss, Oberkochen, Germany) and further fixed by immersion in 4% paraformaldehyde in PB overnight at 4°C. After a thorough rinse in PB, small fragments were collected for transmission electron microscopy (TEM; see below). The remaining tissue was dehydrated in ethanol, cleared in xylene, and embedded in paraffin. For molecular biology assays, animals were anesthetized with ISOflo®/isoflurane (Abbott, Abbott Park, IL) and euthanized by cervical dislocation. BAT and WAT specimens were rapidly removed, snap-frozen in liquid nitrogen, and stored at −80°C until use.

Light microscopy and morphometry

Serial paraffin sections (3 μm thick) were obtained from each adipose depot, placed on glass slides, and dried. Alternate sections were used for hematoxylin and eosin staining to assess morphology, and for immunohistochemical procedures to evaluate tissue protein expression. Adipocyte size was defined as mean adipocyte area (in square micrometers) using a drawing tablet and a morphometric program (Nikon LUCIA IMAGE, Laboratory Imaging, version 4.61; Praha, Czech Republic). Tissue sections were examined with a Nikon Eclipse E800 light microscope, and digital images were captured at 20× with a Nikon DXM 1200 camera (Nikon Instruments S.p.A, Calenzano, Italy). CLS density was determined by counting the total number of (MAC-2-positive) CLSs in each section compared with the total number of adipocytes and was expressed as CLS number/10,000 adipocytes. The CLS index was calculated by dividing CLS density by mean adipocyte size.

Immunohistochemistry

For immunohistochemistry, 3 μm thick paraffin-embedded sections of the fat depots were dewaxed; they were then reacted with 0.3% H_2O_2 (in methanol; 30 min) to block endogenous peroxidase, rinsed with PBS, and incubated in 3% normal serum blocking solution (in PBS; 30 min). Sections were then incubated overnight at 4°C with rat monoclonal anti-MAC-2 antibody (dilution 1:1,500; Cedarlane Laboratories, Burlington, Ontario, Canada), a marker of activated macrophages, or rabbit polyclonal anti-perilipin antibody (dilution 1:300; kindly provided by Dr. A. S. Greenberg, Boston, MA). After a thorough rinse in PBS, sections were incubated in 1:200 v/v horse anti-rat (MAC-2 schedule)

or goat anti-rabbit (perilipin schedule) IgG biotinylated HRP-conjugated secondary antibody solution (Vector Laboratories, Burlingame, CA) in PBS for 30 min. Histochemical reactions were performed using a Vectastain ABC kit (Vector Laboratories) and Sigma Fast 3,3′-diaminobenzidine (Sigma-Aldrich, Vienna, Austria) as the substrate. Sections were counterstained with hematoxylin, dehydrated in ethanol, and mounted in Eukitt® mounting medium (Sigma-Aldrich). Staining was never observed when the primary antibody was omitted. The procedures applied for immunofluorescence and confocal microscopy analysis are described in the supplemental Materials and Methods.

TEM

Small fragments of BAT and WAT from perfused mice were fixed in 2% glutaraldheyde-2% paraformaldehyde in PB for 4 h at room temperature, postfixed in 1% osmium tetroxide, dehydrated in a graded series of acetone, and embedded in an Epon-Araldite mixture. To determine the region of interest, semi-thin sections were cut and stained with toluidine blue. Thin sections were obtained with an MT-X Ultratome (RMC, Tucson, AZ), stained with lead citrate, and examined with a CM10 transmission electron microscope (Philips, Eindhoven, The Netherlands).

RNA isolation and quantitative real-time PCR

Homogenization of frozen BAT and WAT for RNA isolation was performed using an Ultra-Turrax apparatus (IKA, Staufen, Germany) and TRIzol® reagent (Life Technologies, Invitrogen, Vienna, Austria) according to standard protocols. For gene expression analyses, RNA samples were treated with DNase I (Life Technologies, Invitrogen) and reverse transcribed into single-stranded cDNA using a high-capacity reverse transcription kit (Life Technologies, Applied Biosystems, Vienna, Austria). cDNA samples were amplified using Maxima SYBR Green/ROX Master Mix 2x (Fermentas Life Science, St. Leon-Roth, Germany) and primer pairs specific for the target genes (Life Technologies, Invitrogen). The primer sequences are available on request. Real-time PCR was performed on a C1000 thermocycler using the CFX96 real-time system (Bio-Rad Laboratories GmbH, Vienna, Austria). Relative target gene expression was normalized to the ribosomal gene, 36b4, and calculated using the ΔΔCt method (22). The procedures regarding RNA isolation and quantitative (q)PCR of AAKO mice are described in the supplemental Materials and Methods.

XBP-1 splicing assay

Total RNA from BAT was reverse transcribed with a high-capacity reverse transcription kit (Life Technologies, Applied Biosystems) using the reverse Xbp-1 specific primer, reverse 5′-GAGGCAACAGTGTCAGAGTCC-3′, to amplify Xbp-1 cDNA. For Xbp-1 cDNA amplification, conventional PCR was performed using gene-specific primers for Xbp-1 (forward 5′-GAACCAGGAGTTA-AGAACACG-3′ and reverse 5′-GAGGCAACAGTGTCAGAGTCC-3′). PCR reactions were run using Phusion DNA polymerase (Biozym, Vienna, Austria). Primers were designed to amplify both unspliced and unconventionally spliced Xbp-1 in the same reaction. Samples were separated on 3% agarose gel. DNA gels were documented using Image Quant 300 (GE Healthcare Europe GmbH, Vienna, Austria).

DNA isolation and quantitative mitochondrial DNA content analysis

Whole genomic DNA and mitochondrial (mt)DNA were extracted from adipose tissue depots using DNeasy blood and tissue kit (Qiagen Vertriebs GmbH, Vienna, Austria) according to the manufacturer's instructions. mtDNA copy number was determined with quantitative real-time PCR using SYBR green and specific primers for the mitochondrial-encoded cytochrome c oxidase 1 (Mt-Co1) and the single copy nuclear gene, NADH dehydrogenase (ubiquinone) flavoprotein 1 (Ndufv1), as control, as described previously (23). DNA samples were amplified using Maxima SYBR Green/ROX Master Mix 2x (Fermentas Life Science) and gene-specific primer pairs (Life Technologies, Invitrogen). PCR reactions were run on an ABI One Step PLUS system (Life Technologies, Applied Biosystems). Relative mtDNA content was determined by normalizing Mt-Co1 expression values to Ndufv1 and calculated using the ΔΔCt method as described recently (22).

Tissue homogenization and immunoblot analysis

Snap-frozen tissue was homogenized in ice-cold homogenization buffer (0.25 M sucrose, 1 mM EDTA, 1 mM DTT) containing protease inhibitors (20 µg/ml leupeptin, 2 µg/ml antipain, 1 µg/ml pepstatin, pH 7.0) and a phosphatase inhibitor cocktail (Sigma-Aldrich) using a handheld dispenser (Ultra-Turrax). Samples were centrifuged for 30 min at 10,000 or 20,000 g at 4°C. For immunoblotting, specific antibodies against peIF2α and eIF2α were used and GAPDH served as a loading control (all from Cell Signaling Technology, Boston, MA). HRP-conjugated goat anti-rabbit antibody (Vector Laboratories) was used as a secondary antibody. Proteins were visualized using Amersham Hyperfilm ECL (GE Healthcare). Films were scanned (GS-8000; Bio-Rad) and signal density was determined with the Quantity One® program (all from Bio-Rad Laboratories). The target protein signal was normalized to GAPDH and the fold difference of wild-type to *Atgl*-ko samples was determined.

Statistical analysis

Data are expressed as mean ± SEM. Data were tested on normality prior to statistical analysis. Statistical significance was determined between two groups with unpaired two-tailed Student's t-test when normally distributed. Mann-Whitney test was performed when data did not show normality. Statistical significance of more than two groups was analyzed using one-way ANOVA. Group differences were considered significant for $*P < 0.05$, $**P < 0.01$, and $***P < 0.001$. All statistical analyses were performed with Prism 6.0 (GraphPad Software Inc., La Jolla, CA).

RESULTS

Environmental and genetic conditions leading to brown-to-white adipocyte conversion and CLS formation in "whitened" BAT

All raw data of the mean adipocyte area and CLS density of the experimental mouse models examined in the present study are reported in supplemental Table S1.

Warm acclimation. Ambient temperature has a profound influence on body metabolism and energy expenditure, importantly affecting BAT morphology and thermogenesis (13, 14, 24). The impact of ambient temperature on BAT macrophage infiltration was assessed in interscapular BAT (iBAT) and mediastinal BAT (mBAT) from lean C57Bl/6j (B6) mice acclimated to cold (6°C) and warm (28°C) temperatures. In cold-acclimated mice, iBAT and mBAT were composed of typical multilocular adipocytes that exhibited a high degree of UCP-1 immunoreactivity (data not shown). MAC-2 immunohistochemistry demonstrated the absence

of CLSs in iBAT from cold-acclimated mice (**Fig. 1A**, H) and their occasional presence in mBAT (Fig. 1C, H). Brown fat cells from lean mice kept at 28°C, a temperature close to thermoneutrality for rodents, acquired a white-like unilocular adipocyte phenotype. Notably, brown-to-white conversion did not involve significant changes in cell size either in iBAT or in mBAT (Fig. 1G). In contrast, brown-to-white conversion involved increased macrophage infiltration, which led to formation of several CLSs in iBAT (Fig. 1B, H); the density of MAC-2-positive CLSs in mBAT was also increased, even though the difference compared with cold-acclimated mice was not significant (Fig. 1D, H). To establish whether the increased CLS density seen in thermoneutral conditions was confined to BAT, inguinal WAT (iWAT) sections from cold- and warm-acclimated animals were examined. Very few CLSs were detected in iWAT from cold-acclimated mice (Fig. 1E, H), whereas in warm-acclimated animals, there was a significant increase in adipocyte area (Fig. 1G) that was, however, not matched by a significant increase in CLS density (Fig. 1F, H). These data suggest that brown adipocytes converting to a white-like unilocular phenotype at high ambient temperatures have a limited ability to store lipids and grow, and that they become more prone to death and to be cleared by CLSs compared with white adipocytes.

Leptin receptor deficiency. In obese mice, brown adipocytes display a white-like appearance similar to the phenotype found in warm-acclimated mice (13, 24). We therefore investigated to determine whether iBAT from leptin receptor-deficient *db/db* mice showed signs of whitening and CLS formation like warm-acclimated mouse iBAT. Typical brown adipocytes were detected in *db/+* mice (**Fig. 2A**), whereas in *db/db* mice they showed a white-like appearance and a significant size increase (Fig. 2B, E). CLSs were never detected in iBAT from control animals (Fig. 2A, E), whereas they were frequently observed in iBAT from *db/db* mice (Fig. 2B, E).
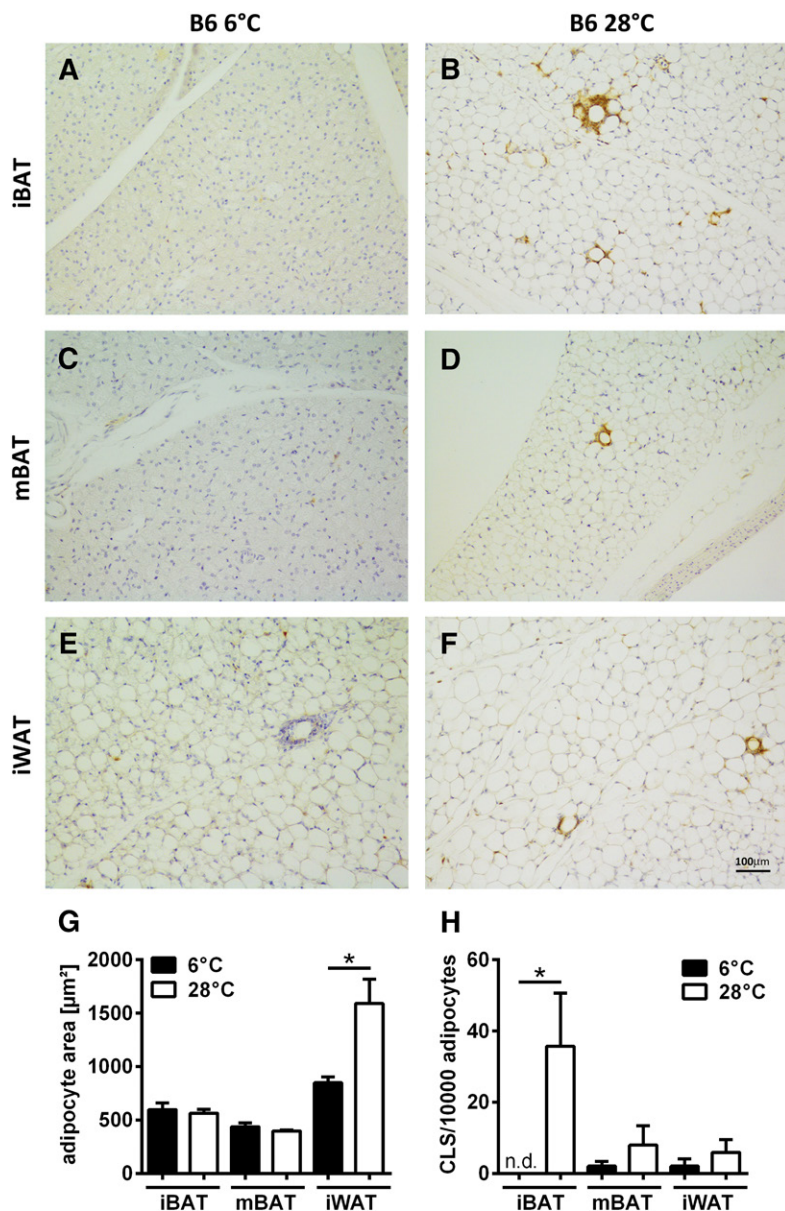

B6 6°C **B6 28°C**

Fig. 1. Warm acclimation induces brown adipocyte whitening and CLS formation. A–F: Representative microscopy pictures of MAC-2-immunostained sections of iBAT, mBAT, and iWAT fat depots from mice kept at 6°C (A, C, E) or 28°C (B, D, F) showing BAT whitening (B, D) and increased adipocyte size and CLS formation in the warm-acclimated animals. G: Comparison of brown and white adipocyte area in iBAT, mBAT, and iWAT from cold-acclimated (6°C) and warm-acclimated (28°C) mice documenting a similar brown adipocyte size in both groups and a significant enlargement of subcutaneous inguinal white adipocytes from warm-acclimated mice (n = 5). H: Comparison of CLS density in cold- and warm-acclimated mice showing that warm acclimation significantly increases CLS density in iBAT, to some extent in mBAT, but not in iWAT (n = 5). Data are expressed as mean ± SEM. Statistical significance was determined using unpaired two-tailed Student's *t*-test for iBAT and the Mann-Whitney test for mBAT and iWAT *$P < 0.05$; n.d., not detectable.
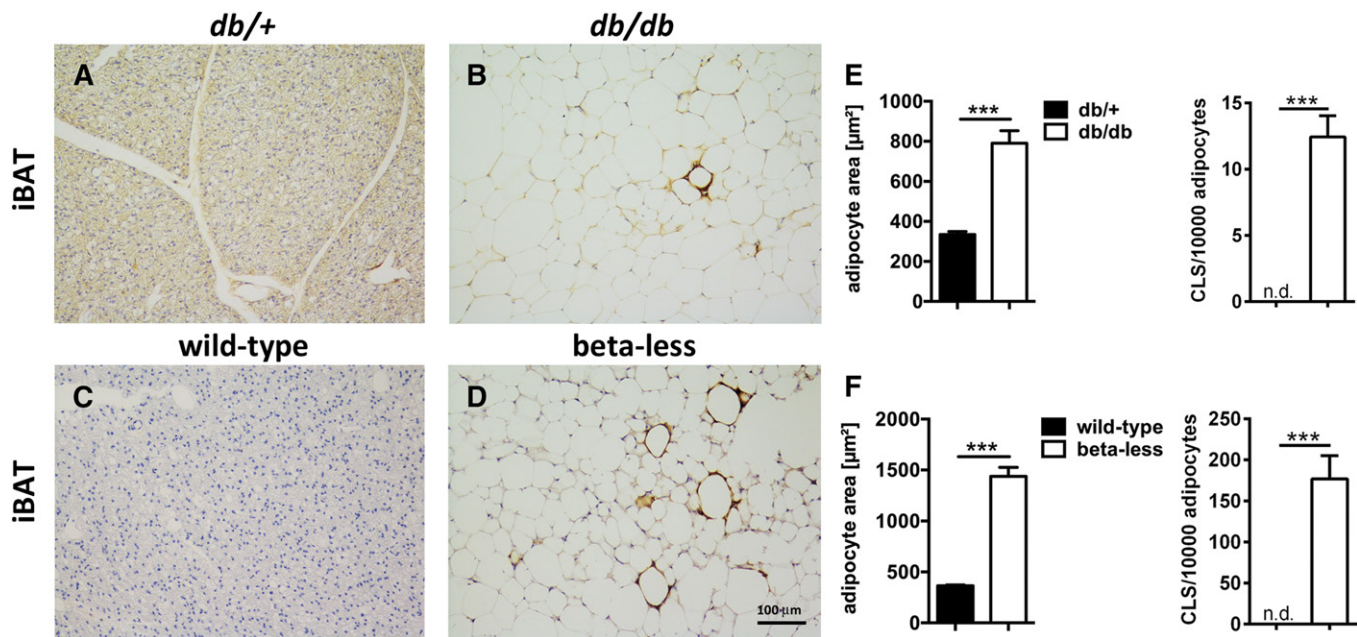
Fig. 2. Increased CLS formation in whitened BAT from *db/db* and β-less mice. A–D: Representative microscopy pictures of MAC-2–immunostained sections of iBAT from genetically diabetic (*db/db*) and β-adrenergic signaling (β-less)-deficient mice and their respective controls showing whitened, enlarged brown adipocytes, and increased CLS formation in both models. E, F: Increased interscapular brown adipocyte area and iBAT CLS density in both *db/db* (E) and β-less (F) mice compared with the respective controls (n = 5). Data are expressed as mean ± SEM. Statistical significance was determined by using unpaired two-tailed Student's *t*-test; ****P* < 0.001.

The β-less mice. BAT-to-WAT conversion in warm-acclimated and obese mice is held to be mediated by low activity of the sympathetic nervous system (13, 14, 24), whose tonic noradrenergic signaling is required for brown phenotype maintenance (25–27). To explore the whitening process in the absence of the adrenergic stimulus, iBAT morphology and cell composition were studied in β-less mice (21). In these β-less mice, BAT exhibited a marked white-like appearance and adipocyte hypertrophy (Fig. 2D, F) compared with BAT of control mice (Fig. 2C, F). In line with the above-reported findings, BAT from control mice did not contain CLSs (Fig. 2C, F), whereas whitened BAT from β-less mice was characterized by a large number of CLSs (Fig. 2D, F).

Atgl deletion. ATGL is a key enzyme for lipolysis, the intracellular hydrolysis of triglycerides. Global *Atgl* ko induces mild obesity and adipose tissue expansion, even in mice fed a standard chow diet (19). ATGL activity is crucial for normal BAT morphology and function because its deletion leads to severe BAT hypertrophy and to the acquisition of a WAT-like phenotype (19, 28). However, it is unclear whether BAT whitening in *Atgl*-ko mice also involves changes in macrophage infiltration and CLS formation. To gain insight into the question, adipocyte size and CLS density were assessed in iBAT, mBAT, and iWAT from wild-type and *Atgl*-ko mice kept in standard laboratory conditions. In wild-type mice, brown and white adipocyte appearance and size were normal in all three depots, whereas CLSs were rare in iBAT (**Fig. 3A**, H) and absent in mBAT (Fig. 3C, H) and iWAT (Fig. 3E, H). As expected (19, 28), genetic *Atgl* ablation involved brown-to-white-like conversion in brown depots and an important size increase of

both brown and white adipocytes (Fig. 3G). Interestingly, the size of transformed iBAT and mBAT brown adipocytes from these mice was not significantly different from the size of iWAT white adipocytes (Fig. 3G). In striking contrast, CLS density was very high in iBAT (Fig. 3B, H), high in mBAT (Fig. 3D, H), and low in iWAT (Fig. 3F, H). In this model of BAT whitening, enlarged white-like brown adipocytes therefore die in large numbers when they reach a size and lipid content that are still tolerated by white adipocytes. In epididymal WAT (eWAT) and mesenteric WAT visceral fat, *Atgl* deficiency involved an enlargement of white adipocytes associated with increased CLS density compared with control mice (supplemental Fig. S1).

Brown adipocyte death and CLS index

To estimate the number of healthy versus dysfunctional, or dying, whitened brown adipocytes in iBAT, we assessed the immunohistochemical expression of perilipin, a widely used marker of adipocyte viability (29–31). The brown adipocytes from control mice were strongly and consistently perilipin-immunoreactive (**Fig. 4A**). In contrast, perilipin expression was low, very low, or absent in a variable number of whitened brown adipocytes from the experimental groups. In particular, slightly positive or negative adipocytes were about 5% in warm-acclimated mice, about 5–10% in *db/db* mice, about 20–30% in β-less mice, and about 30–40% in *Atgl*-ko mice (Fig. 4B). As also shown by double labeling experiments and confocal microscopy analysis (supplemental Fig. S2), specific perilipin staining was never detected in CLSs (Fig. 4C), which confirmed that they were formed of brown adipocyte debris, mainly lipids, surrounded by macrophages. Notably, perilipin staining
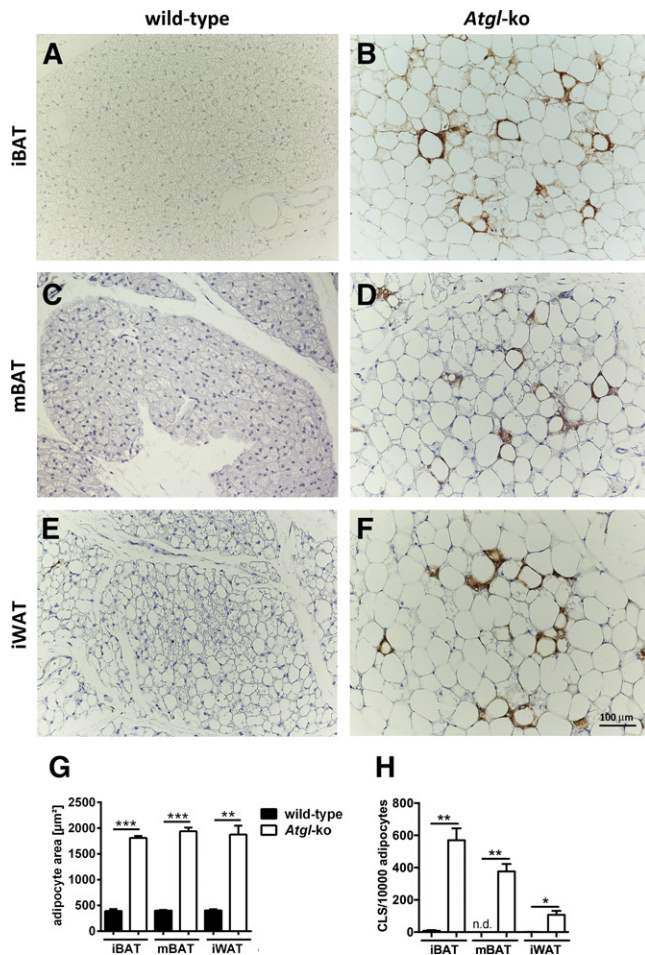
Fig. 3. *Atgl* deficiency promotes adipocyte hypertrophy and CLS formation in WAT and BAT. A–F: MAC-2-immunostained sections from iBAT, mBAT, and iWAT fat depots from wild-type (A, C, E) and *Atgl*-ko (B, D, F) mice, showing BAT whitening (B, D), hypertrophic adipocytes, and increased CLS formation in *Atgl*-ko mice. G: Comparison of brown and white adipocyte area showing enlarged adipocytes in all adipose depots from *Atgl*-deficient animals (n = 3). H: Comparison of CLS density in *Atgl*-ko and wild-type mice showing that *Atgl* deletion involves a significant increase in CLS density in all depots from the former mice (n = 3). Data are expressed as mean ± SEM. Statistical significance was determined using unpaired two-tailed Student's t-test; *$P < 0.05$; **$P < 0.01$; ***$P < 0.001$.

was detected around small cytoplasmic lipid droplets in some endothelial cells of parenchymal capillaries from the whitened iBAT of *Atgl*-ko mice (Fig. 4D).

The above data suggest that lipid overload and/or functional inhibition induce brown adipocyte conversion to a white-like phenotype, which makes them highly prone to death and to be cleared by macrophages. Given that cell size is strongly involved in inducing such proneness to death (6, 7, 12), all mouse models were compared by their CLS index, i.e., the ratio between CLS density (CLSs/10,000 adipocytes) and the respective mean adipocyte area (in square micrometers). Interestingly, the CLS index was highest in *Atgl*-ko mouse iBAT (**Fig. 5**). ATGL deletion thus seems to be the most robust model to study the mechanisms and metabolic consequences of brown adipocyte whitening and CLS formation.
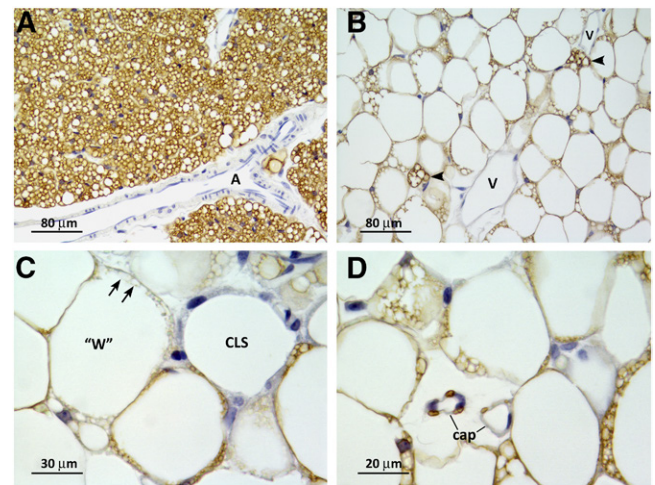

Fig. 4. Perilipin immunostaining in *Atgl*-ko mouse iBAT. A: In wild-type animals, brown adipocytes are strongly positive for perilipin, which is localized around the small lipid droplets. B–D: In *Atgl*-ko mice, the vast majority of whitened brown adipocytes exhibit reduced perilipin immunostaining, while some multilocular adipocytes (B, arrowheads) retain a fairly strong perilipin immunopositivity. At higher magnification (C), perilipin staining is absent in a CLS and in an adjacent whitened brown adipocyte ("W"), where even its small lipid droplets are completely negative (arrows). D: Two capillaries (cap) contain endothelial cells filled with some perilipin-positive small lipid droplets. A, artery; V, vein.

Ultrastructure of whitened BAT from *Atgl*-deficient mice

TEM examination of iBAT specimens from control mice revealed typical brown adipocytes filled with several small lipid droplets and containing numerous large mitochondria packed with laminar cristae (**Fig. 6A**). In *Atgl*-ko mice, the brown adipocytes were enlarged and their cytoplasm contained large and coalescing lipid droplets and numerous mitochondria (Fig. 6B). The majority of examined mitochondria still contained packed laminar cristae (Fig. 6D), but some mitochondria exhibited signs of degeneration characterized by the absence of cristae in restricted portions of the organelle (inset of Fig. 6B). Some whitened brown adipocytes exhibited dilated ER and cholesterol crystals (Fig. 6C). In the extracellular space, an increased number of collagen fibrils was found around the whitened brown adipocytes (Fig. 6C) and small lipid droplets were occasionally detected in the endothelial capillary wall (Fig. 6D), in line with perilipin immunostaining observed on light microscopy. All sections contained a large number of macrophages, some of which were clustered around adipocyte debris, sometimes forming syncytia (Fig. 6E). On the whole, the ultrastructure of the CLSs found in *Atgl*-ko mouse iBAT was very similar to that seen in subcutaneous and visceral WAT from obese animals (6, 7), suggesting that CLSs are a morphological "hallmark" of both white and brown adipocyte death.

Whitening of brown adipocytes in *Atgl*-deficient mice induces BAT inflammation and NLRP3 inflammasome activation

Increased CLS density is usually directly proportional to increased expression of inflammatory marker genes, as previously described (4–7). Therefore, we measured
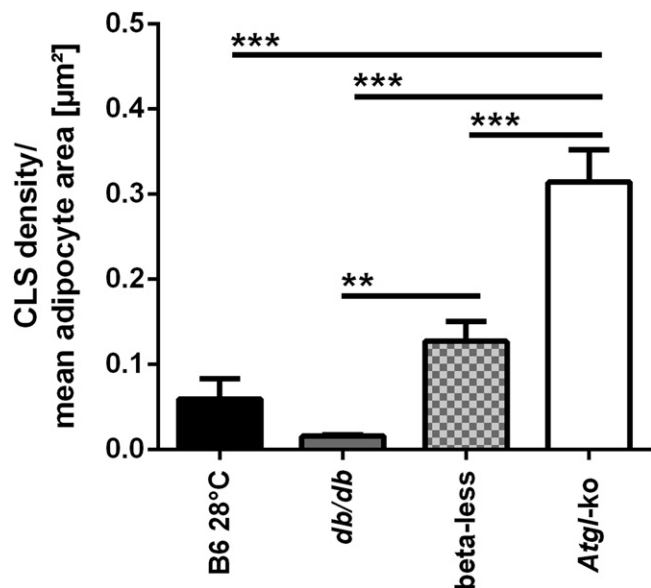
Fig. 5. The CLS index. Comparison of the CLS indices (CLS density/mean adipocyte area) calculated in iBAT from the different mouse models examined in the study shows the highest value in *Atgl*-ko mice. Data are expressed as mean ± SEM. Statistical significance was determined by one-way ANOVA and Tukey's multiple comparison post hoc test; **$P < 0.01$; ***$P < 0.001$.

inflammatory and inflammasome marker expression in *Atgl*-ko mice. In line with the morphological data, the high CLS density found in BAT from *Atgl*-ko mice was associated with a robust inflammatory response in iBAT, which was reflected in an increased abundance of the mRNA of classic adipose tissue inflammation markers, such as F4/80, Tnfα, and Mcp-1 (**Fig. 7A**). Interestingly, markers for M2 macrophage polarization (IL-10 and Mgl1), which indicate the presence of M2 macrophages, were also significantly upregulated in *Atgl*-ko mouse iBAT (Fig. 7A). Finally, induction of the expression of NLRP3 inflammasome markers, such as Casp-1 and IL-18, in iBAT of *Atgl*-ko mice (Fig. 7B) suggests that inflammasome activation might be the driver of brown fat inflammation and CLS formation in these animals, as previously hypothesized for obese WAT (12).

BAT inflammation in *Atgl*-deficient mice is independent of ER stress and mitochondrial dysfunction

ER stress, mitochondrial dysfunction, and the consequent presence of large amounts of reactive oxygen species in adipose tissue are held to be involved in adipocyte death and in the development of adipose tissue inflammation and dysfunction (10, 11, 32–34). Therefore, established markers of ER stress and mitochondrial dysfunction were measured to assess whether either or both mechanisms might underpin inflammasome activation and inflammation in whitened *Atgl*-ko mouse iBAT. ER stress induction was analyzed by measuring the mRNA abundance of several members of the unfolded protein response, such as Grp78/Bip, Xbp-1 splicing, and eIF2α phosphorylation. However, there were no changes in Xbp-1 splicing (**Fig. 8A**), Grp78/Bip and Chop expression (Fig. 8B), or eIF2α phosphorylation (Fig. 8C). Similar results were obtained

from the analyses of mitochondrial degeneration markers because neither cytochrome c release nor mtDNA content were altered in iBAT from *Atgl*-ko mice compared with controls (Fig. 8D, E). Finally, the expression of the oxidative stress marker, catalase, was not altered (Fig. 8F), whereas Gpx1 only moderately increased (Fig. 8G) in iBAT from *Atgl*-deficient mice.

iBAT from AAKO mice contains numerous CLSs and shows signs of inflammation

To exclude the possibility that the phenotype found in *Atgl*-deficient mouse BAT was due to the lack of ATGL in macrophages or in other cell types, the analysis was extended to AAKO mice, where adiponectin-driven Cre expression was used to selectively target *Atgl* deletion in white and brown adipocytes (20). As already reported (20), the iBAT of AAKO mice exhibited a marked white-like appearance. Both iBAT and eWAT from these mice exhibited a significant increase in adipocyte size and CLS density compared with wild-type controls (supplemental Fig. S3); notably, the increase in CLS density was especially marked in iBAT. The expression of some inflammatory markers, including F4/80, Chop/Ddit, GPX1, and Casp-1, was significantly increased in the iBAT of AAKO mice compared with control mice (supplemental Fig. S3). NLRP3 mRNA was not detected in the iBAT of wild-type control mice, but showed a low level of expression in AAKO mice. Interestingly, no signs of inflammasome activation were detected in the eWAT of AAKO mice (supplemental Fig. S3). Altogether, these data show that selective ATGL deletion in adipocytes is able to induce cell hypertrophy and death and to lead to macrophage infiltration and CLS formation that are particularly pronounced in BAT, where these processes may ultimately sustain tissue inflammation.

DISCUSSION

Obesity is a multifactorial disease resulting from a chronic imbalance between food intake and energy expenditure. An enduring and sustained positive energy balance leads to the progressive enlargement of subcutaneous and visceral WAT depots, due to an increase in white adipocyte number (hyperplasia) as well as size (hypertrophy). When the adipose organ is no longer capable of buffering the excess nutrients, ectopic lipid deposition occurs in liver, muscle, heart, and pancreas (35–37). Importantly, the enlarged obese WAT develops a low-grade inflammatory state (4, 5). Histologically, obese WAT inflammation is marked by the presence of CLSs, where aggregates of macrophages surround dead adipocytes to clear the extracellular space of adipocyte debris, especially the large lipid droplets (4–7). Stressed and dysfunctional obese adipocytes and dead adipocytes trigger the production of proinflammatory adipokines and chemoattractants, which in turn instigate inflammatory cell infiltration, eventually leading to a chronic inflammatory state (8, 35, 38). The consequent upregulation of inflammatory cytokines and downregulation of anti-inflammatory adipokines are crucial to induce the
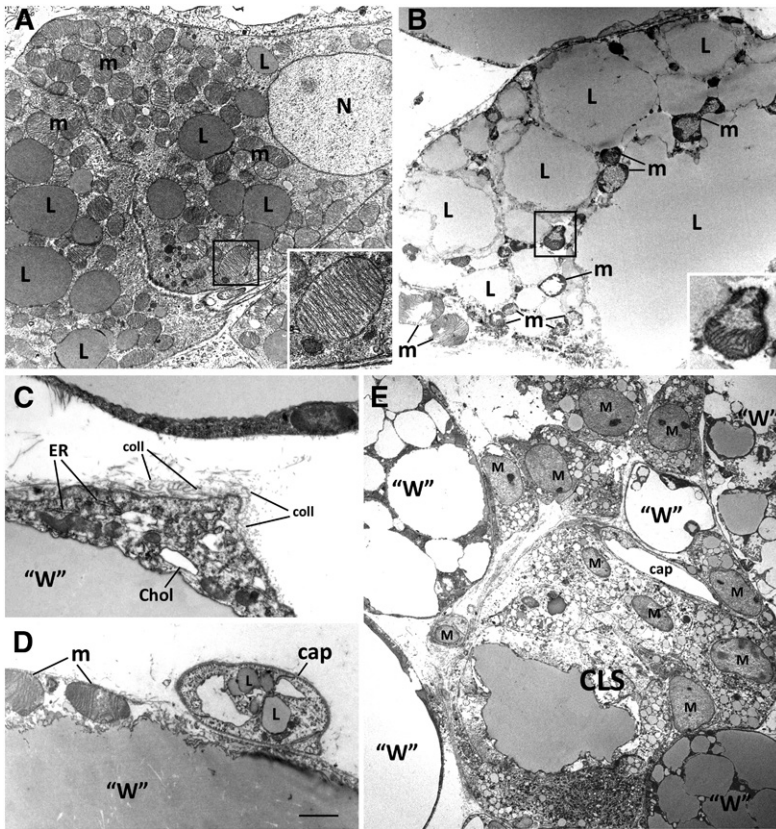
Fig. 6. - TEM of whitened brown adipocytes from *Atgl*-ko mice. A: In wild-type animals, brown adipocytes show their typical ultrastructural appearance and contain several small lipid droplets (L) and numerous large mitochondria filled with parallel cristae (m); one typical brown mitochondrion is shown in the inset. B: An enlarged brown adipocyte from an *Atgl*-ko mouse contains large and coalescing lipid droplets (L) and mitochondria (m) that, in addition to the typical packed and parallel cristae, show degenerating areas (compare the inset of B with the inset of A). C: High magnification of the cytoplasmic rim of a whitened brown adipocyte ("W") from an *Atgl*-ko mouse containing dilated ER and a cholesterol crystal (Chol). Note the abundance of collagen fibrils (coll) in the extracellular space. D: Small lipid droplets (L) are seen in the endothelial cells of a capillary (cap) found in close proximity to an *Atgl*-ko mouse whitened brown adipocyte ("W"), where mitochondria (m) with degenerating areas are also visible. E: In the iBAT of an *Atgl*-ko mouse, several macrophages (M) are detected among brown adipocytes ("W") showing different degrees of whitening; some macrophages are arranged into a CLS. Insets are enlargements of the corresponding framed areas. N, nucleus. Scale bars: 1.5 μm (A), 0.4 μm (inset of A); 0.9 μm (B), 0.3 (inset of B); 0.4 μm (C, D); 3 μm (E).

major metabolic and cardiovascular consequences of obesity (35, 38, 39).

While numerous studies have explored the morphological and pathophysiological aspects of obese WAT, especially visceral WAT, whose involvement is linked to the more severe morbid consequences of obesity (40), obese BAT has not been extensively investigated.

In genetic or acquired obesity, BAT function declines and the tissue acquires a white-like appearance (whitening). Histologically, whitened brown adipocytes show a unilocular rearrangement of their lipid content but, as demonstrated by TEM, their cytoplasm still contains brown-like typical mitochondria filled with numerous packed cristae (13). By immunohistochemistry, whitened brown adipocytes retain a weak mitochondrial UCP1 immunoreactivity, but also begin to express leptin (18, 41), the typical white adipocyte hormone, and reduce the expression of many classic brown genes (42). Even though de novo white adipocyte formation and/or infiltration of adjacent white adipocytes, which are usually located at the periphery of BAT lobules, could contribute to BAT whitening, these data suggest that in some conditions involving lipid overload and/or inhibited oxidation, brown adipocytes can directly convert to white-like adipose cells with few or no thermogenic properties (43, 44).

Importantly, data from rodents and humans stress that the development of obesity and its complications largely depends on the balance between WAT, the main energy store
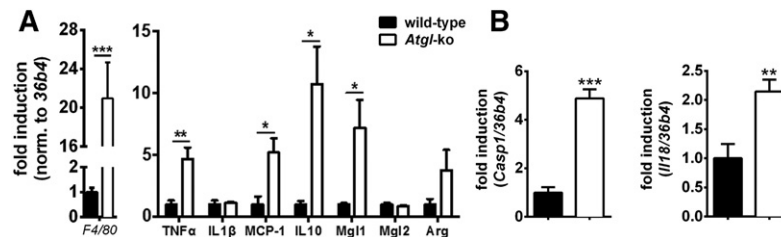

Fig. 7. iBAT of *Atgl*-ko mice exhibits increased expression of inflammatory cytokines and NLRP3 inflammasome activation. A: Determination of the relative mRNA abundance of F4/80, Tnfα, IL-1β, Mcp-1, IL-10, Mgl1, Mgl2, and Arg in iBAT from wild-type and *Atgl*-ko mice showing higher expression levels in the latter mice (n = 5–6 per genotype, refed mice). B: The expression of inflammasome markers, Casp-1 and IL-18, is upregulated in *Atgl*-ko mouse iBAT (n = 6, refed mice). The mRNA levels of the inflammation and inflammasome markers were measured by quantitative real-time PCR. Target gene abundance was normalized to 36b4 and expressed relative to wild-type levels of each marker. Data are expressed as mean ± SEM. Statistical significance between groups was calculated using unpaired two-tailed Student's *t*-test or Mann-Whitney test for Mgl1 mRNA abundance and is expressed as: *$P < 0.05$; **$P < 0.01$; ***$P < 0.001$.
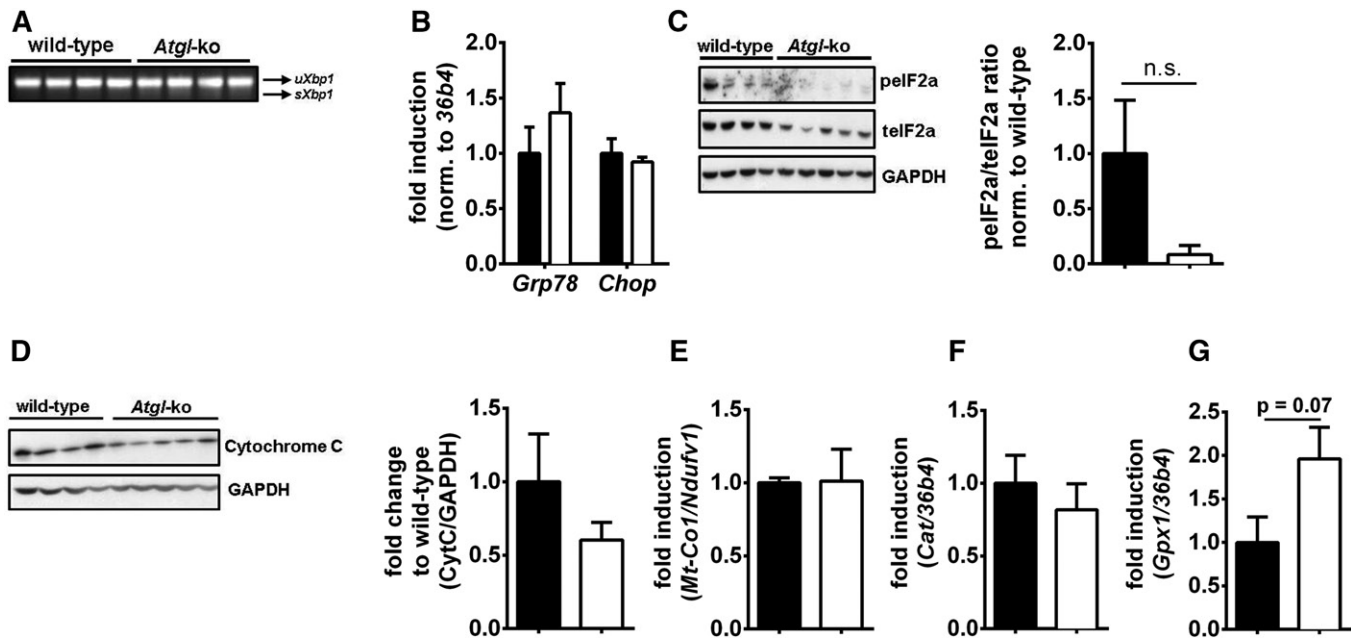
Fig. 8. iBAT from *Atgl*-ko mice does not show signs of ER stress or mitochondrial destruction. Assessment of ER stress markers, such as Xbp-1 splicing (A), Grp78 and Chop mRNA levels (B), and eIF2a phosphorylation (C), shows no difference between wild-type and *Atgl*-ko mice, thus excluding ER stress in iBAT from *Atgl*-ko mice (n = 4, refed mice). Cytochrome c release in iBAT lysates (D) and qPCR analysis of iBAT mitochondrial (mt) DNA content (E): the relative abundance of the mtDNA-encoded gene Mt-Co1 was measured by qPCR, normalized to the nuclear single copy gene, Ndufv1, and expressed relative to wild-type levels (n = 4–6, refed mice), showing that mitochondrial integrity is not affected in *Atgl*-ko mouse iBAT. The mRNA abundance of catalase (F) and Gpx1 (G) in *Atgl*-ko mouse iBAT, which reflect oxidative stress, remained unchanged (n = 5–6, refed mice). Relative mRNA levels were measured by quantitative real-time PCR. Target gene abundance was normalized to 36b4 and expressed relative to wild-type levels of each marker. Data are expressed as mean ± SEM. Statistical significance between groups was calculated with unpaired two-tailed Student's *t*-test or Mann-Whitney test for Gpx1 mRNA abundance.

of the body, and BAT, whose task is to produce energy via nonshivering thermogenesis. For instance, in mice, BAT ablation leads to obesity (45), ectopic UCP1 expression in WAT results in resistance to obesity (46), and reduced BAT-dependent nonshivering thermogenesis impairs insulin sensitivity (47). In humans, a reduced brown adipose phenotype is associated with insulin resistance (48), and obese individuals show BAT atrophy associated with visceral fat accumulation, aging, and hyperglycemia (49), suggesting that defective BAT function may induce and/or exacerbate obesity and its complications.

However, the fate of whitened brown adipocytes and whether whitened BAT develops inflammation, possibly contributing to the systemic inflammatory state found in obesity, have not been explored in depth. The models of energy imbalance used in the present study suggest that whitening may be caused by leptin receptor deficiency, absence of β-adrenergic signaling to brown adipocytes, or lipase deficiency. In each of these conditions, brown fat whitening results in macrophage infiltration, adipocyte death, and CLS formation. Notably, the most marked effect of brown-to-white conversion was seen in *Atgl*-deficient mice (19, 28), which, even in normal temperature and dietary conditions, developed enlarged brown adipocytes and BAT inflammation with increased CLS formation and expression of inflammatory marker genes, such as Tnfα and Mcp-1. These data are consistent with the findings of recent studies of whitened BAT from diet-induced obese mice, which have reported macrophage recruitment to

BAT and increased expression of proinflammatory mediators (47, 50–52). Some ultrastructural aspects of the whitened brown adipocytes of *Atgl*-ko mice (such as cholesterol crystals) and the NLRP3 inflammasome activation (increased expression of Casp-1 and IL-18) suggest that brown adipocytes may undergo pyroptotic cell death, as described in hypertrophic and dysfunctional white adipocytes (12). ER stress and mitochondrial dysfunction have been implicated in causing adipocyte dysfunction and death and adipose tissue inflammation (10, 11, 33, 34). Even though TEM data showed ER dilatation and mitochondrial degeneration in some whitened brown adipocytes, no clear evidence of ER stress or mitochondrial dysfunction in the iBAT of *Atgl*-ko mice was found on a molecular level. Therefore, in our study, few effects of BAT whitening on mitochondrial function occur in *Atgl*-ko mice, in accordance with the recent demonstration that iBAT retains fairly normal thermogenic activity in AAKO mice (53). However, a previous experiment had clearly identified mitochondrial dysfunction in the cardiac muscle of ATGL-ko mice (54). A close involvement of mitochondria in brown adipocyte whitening is also suggested by a recent study showing that loss of the scaffold protein, p62, in adipose tissue leads to BAT whitening, impaired nonshivering thermogenesis, and obesity that are linked to mitochondrial dysfunction (55). Impaired vascularization in vascular endothelium growth factor (VEGF)-ko mice has also been shown to be a primary factor leading to BAT whitening, which was characterized by lipid accumulation, mitochondrial

dysfunction, and impaired noradrenergic signaling (56). In addition, it has been suggested that abnormal amounts of intracellular fatty acids, as could occur in ATGL-depleted adipocytes, can activate the NLRP3 inflammasome directly (57). Clearly, different molecular mechanisms can contribute to BAT whitening and obesity-related BAT dysfunction, and the primary cellular mechanism leading to whitening in *Atgl*-ko mice remains to be determined. However, our data suggest that enlargement or simply the acquirement of a spherical shape by whitened brown adipocytes that also show prominent organelle alterations by TEM may be sufficient to induce inflammasome activation in these cells, even in the absence of biochemically detectable signs of ER stress and mitochondrial dysfunction from the whole BAT depot.

The present data show that the histological appearance of brown and white adipocyte death is very similar at both light and electron microscopy. Indeed, brown and white stressed and dysfunctional adipocytes both appear to induce macrophage recruitment and to die, giving rise to CLSs. Thus, CLSs create the tissue microenvironment where adipocyte debris can adequately be resorbed. Importantly, they are also found in healthy brown and white fat, albeit in very small number [(6, 7) and present results]; therefore, CLSs are not necessarily a pathological feature, but one that may reflect normal adipocyte turnover. In this connection, numerous CLSs were unexpectedly detected in the whitened BAT of mice exposed to warm acclimation, which is not a pathological condition, but a condition that induces a significant size increase, further underlining the importance of normal morphology maintenance for adipocyte viability. This raises the interesting hypothesis of a "physiological" role of CLSs in normal fat turnover, and of the existence of "molecularly different" CLSs that in some instances are proinflammatory, while others are involved in normal homeostatic fat processes.

According to all the models of energy imbalance and obesity that were explored in this study, brown adipocytes show a substantial death rate. Thus, we can hypothesize that in lipid overload conditions brown and white adipocytes display a strikingly different behavior. White adipocytes, such as those from subcutaneous depots, have an outstanding ability to expand and reach a large critical death size, whereas whitened brown adipocytes have a more limited lipid storage capacity and a smaller critical death size, which results in a greater proneness to death. This mechanism may be of crucial importance for the pathophysiology of human obesity because, as suggested by NLRP3 inflammasome activation in whitened BAT of *Atgl*-ko and AAKO mice, the death of brown adipocytes beyond a certain threshold may induce BAT inflammation; this process, combined with WAT inflammation, may compound the systemic inflammatory state typical of obesity. As documented by fluorodeoxyglucose positron emission tomography studies combined with computed tomography, metabolically active BAT is found in humans at visceral sites, mainly around the aorta and the proximal portion of its thoracic and abdominal branches (49, 58, 59). Chronic exposure to an obesogenic environment may induce whitening of these brown adipocytes which, given their high propensity to die, may thus provide a major contribution to obesity-related inflammation, offering a novel explanation for the strong role of visceral fat in determining the most adverse metabolic and cardiovascular outcomes of obesity.

REFERENCES

1. NCD Risk Factor Collaboration (NCD-RisC). 2016. Trends in adult body-mass index in 200 countries from 1975 to 2014: a pooled analysis of 1698 population-based measurement studies with 19.2 million participants. *Lancet.* **387:** 1377–1396.
2. Klöting, N., M. Fasshauer, A. Dietrich, P. Kovacs, M. R. Schön, M. Kern, M. Stumvoll, and M. Blüher. 2010. Insulin-sensitive obesity. *Am. J. Physiol. Endocrinol. Metab.* **299:** E506–E515.
3. Centers for Disease Control and Prevention. 2011. National diabetes fact sheet: national estimates and general information on diabetes and prediabetes in the United States, 2011. Atlanta (GA): US Department of Health and Human Services, Centers for Disease Control and Prevention.
4. Weisberg, S. P., D. McCann, M. Desai, M. Rosenbaum, R. L. Leibel, and A. W. Ferrante. 2003. Obesity is associated with macrophage accumulation in adipose tissue. *J. Clin. Invest.* **112:** 1796–1808.
5. Xu, H., G. T. Barnes, Q. Yang, G. Tan, D. Yang, C. J. Chou, J. Sole, A. Nichols, J. S. Ross, L. A. Tartaglia, et al. 2003. Chronic inflammation in fat plays a crucial role in the development of obesity related insulin resistance. *J. Clin. Invest.* **112:** 1821–1830.
6. Cinti, S., G. Mitchell, G. Barbatelli, I. Murano, E. Ceresi, E. Faloia, S. Wang, M. Fortier, A. S. Greenberg, and M. S. Obin. 2005. Adipocyte death defines macrophage localization and function in adipose tissue of obese mice and humans. *J. Lipid Res.* **46:** 2347–2355.
7. Murano, I., G. Barbatelli, V. Parisani, C. Latini, G. Muzzonigro, M. Castellucci, and S. Cinti. 2008. Dead adipocytes, detected as crown-like structures, are prevalent in visceral fat depots of genetically obese mice. *J. Lipid Res.* **49:** 1562–1568.
8. Guilherme, A., J. V. Virbasius, V. Puri, and M. P. Czech. 2008. Adipocyte dysfunctions linking obesity to insulin resistance and type 2 diabetes. *Nat. Rev. Mol. Cell Biol.* **9:** 367–377.
9. Bartelt, A., and J. Heeren. 2014. Adipose tissue browning and metabolic health. *Nat. Rev. Endocrinol.* **10:** 24–36.
10. Gregor, M. F., and G. S. Hotamisligil. 2007. Adipocyte stress: the endoplasmic reticulum and metabolic disease. *J. Lipid Res.* **48:** 1905–1914.
11. Kusminski, C. M., and P. E. Scherer. 2012. Mitochondrial dysfunction in white adipose tissue. *Trends Endocrinol. Metab.* **23:** 435–443.
12. Giordano, A., I. Murano, E. Mondini, J. Perugini, A. Smorlesi, I. Severi, R. Barazzoni, P. E. Scherer, and S. Cinti. 2013. Obese adipocytes show ultrastructural features of stressed cells and die of pyroptosis. *J. Lipid Res.* **54:** 2423–2436.
13. Cinti, S. 1999. The Adipose Organ. Kurtis, Milan, Italy.
14. Cannon, B., and J. Nedergaard. 2004. Brown adipose tissue: function and physiological significance. *Physiol. Rev.* **84:** 277–359.
15. Murano, I., G. Barbatelli, A. Giordano, and S. Cinti. 2009. Noradrenergic parenchymal nerve fiber branching after cold acclimatisation correlates with brown adipocyte density in mouse adipose organ. *J. Anat.* **214:** 171–178.
16. Vitali, A., I. Murano, M. C. Zingaretti, A. Frontini, D. Ricquier, and S. Cinti. 2012. The adipose organ of obesity-prone C57BL/6J mice is composed of mixed white and brown adipocytes. *J. Lipid Res.* **53:** 619–629.
17. Sbarbati, A., M. Morroni, C. Zancanaro, and S. Cinti. 1991. Rat interscapular brown adipose tissue at different ages: a morphometric study. *Int. J. Obes.* **15:** 581–587.
18. Cinti, S., R. C. Frederich, M. C. Zingaretti, R. De Matteis, J. S. Flier, and B. B. Lowell. 1997. Immunohistochemical localization of leptin and uncoupling protein in white and brown adipose tissue. *Endocrinology.* **138:** 797–804.
19. Haemmerle, G., A. Lass, R. Zimmermann, G. Gorkiewicz, C. Meyer, J. Rozman, G. Heldmaier, R. Maier, C. Theussl, S. Eder, et al. 2006. Defective lipolysis and altered energy metabolism in mice lacking adipose triglyceride lipase. *Science.* **312:** 734–737.
20. Schoiswohl, G., M. Stefanovic-Racic, M. N. Menke, R. C. Wills, B. A. Surlow, M. K. Basantani, M. T. Sitnick, L. Cai, C. F. Yazbeck, D. B.

Stolz, et al. 2015. Impact of reduced ATGL-mediated adipocyte lipolysis on obesity-associated insulin resistance and inflammation in male mice. *Endocrinology.* **156:** 3610–3624.

21. Bachman, E. S., H. Dhillon, C. Y. Zhang, S. Cinti, C. A. Bianco, K. B. Kobilka, and B. B. Lowell. 2002. betaAR signaling required for diet-induced thermogenesis and obesity resistance. *Science.* **297:** 843–845.

22. Livak, K. J., and T. D. Schmittgen. 2001. Analysis of relative gene expression data using real-time quantitative PCR and the 2(-Delta Delta C(T)) method. *Methods.* **25:** 402–408.

23. Amthor, H., R. Macharia, R. Navarrete, M. Schuelke, S. C. Brown, A. Otto, T. Voit, F. Muntoni, G. Vrbóva, T. Partridge, et al. 2007. Lack of myostatin results in excessive muscle growth but impaired force generation. *Proc. Natl. Acad. Sci. USA.* **104:** 1835–1840.

24. Frontini, A., and S. Cinti. 2010. Distribution and development of brown adipocytes in the murine and human adipose organ. *Cell Metab.* **11:** 253–256.

25. Bartness, T. J., and G. N. Wade. 1984. Effects of interscapular brown adipose tissue denervation on body weight and energy metabolism in ovariectomized and estradiol-treated rats. *Behav. Neurosci.* **98:** 674–685.

26. Dulloo, A. G., and D. S. Miller. 1984. Energy balance following sympathetic denervation of brown adipose tissue. *Can. J. Physiol. Pharmacol.* **62:** 235–240.

27. Klingenspor, M., A. Meywirth, S. Stohr, and G. Heldmaier. 1994. Effect of unilateral surgical denervation of brown adipose tissue on uncoupling protein mRNA level and cytochrom-c-oxidase activity in the Djungarian hamster. *J. Comp. Physiol. B.* **163:** 664–670.

28. Ahmadian, M., M. J. Abbott, T. Tang, C. S. S. Hudak, Y. Kim, M. Bruss, M. K. Hellerstein, H-Y. Y. Lee, V. T. Samuel, G. I. Shulman, et al. 2011. Desnutrin/ATGL is regulated by AMPK and is required for a brown adipose phenotype. *Cell Metab.* **13:** 739–748.

29. Souza, S. C., L. M. de Vargas, M. T. Yamamato, P. Line, M. D. Franciosa, L. G. Moss, and A. S. Greenberg. 1998. Overexpression of perilipin A and B blocks the ability of tumor necrosis factor to increase adipocyte lipolysis in 3T3-L1 adipocytes. *J. Biol. Chem.* **273:** 24665–24669.

30. Londos, C., D. Brasaemle, C. Schultz, J. Segrest, and A. Kimmel. 1999. Perilipins, ADRP, and other proteins that associate with intracellular neutral lipid droplets in animal cells. *Semin. Cell Dev. Biol.* **10:** 51–58.

31. Pajvani, U. B., M. E. Trujillo, T. P. Combs, P. Iyengar, L. Jelicks, K. A. Roth, R. N. Kitsis, and P. E. Scherer. 2005. Fat apoptosis through targeted activation of caspase 8: a new mouse model of inducible and reversible lipoatrophy. *Nat. Med.* **11:** 797–803.

32. Pagliassotti, M. J., P. Y. Kim, A. L. Estrada, C. M. Stewart, and C. L. Gentile. 2016. Endoplasmic reticulum stress in obesity and obesity-related disorders: An expanded view. *Metabolism.* **65:** 1238–1246.

33. Hotamisligil, G. S. 2017. Inflammation, metainflammation and immunometabolic disorders. *Nature.* **542:** 177–185.

34. Bhatti, J. S., G. K. Bhatti, and P. H. Reddy. 2017. Mitochondrial dysfunction and oxidative stress in metabolic disorders - a step towards mitochondria-based therapeutic strategies. *Biochim. Biophys. Acta.* **1863:** 1066–1077.

35. Smith, U. 2015. Abdominal obesity: a marker of ectopic fat accumulation. *J. Clin. Invest.* **125:** 1790–1792.

36. Begovatz, P., C. Koliaki, K. Weber, K. Strassburger, B. Nowotny, P. Nowotny, K. Müssig, J. Bunke, G. Pacini, J. Szendrödi, et al. 2015. Pancreatic adipose tissue infiltration, parenchymal steatosis and beta cell function in humans. *Diabetologia.* **58:** 1646–1655.

37. Carobbio, S., S. Rodriguez-Cuenca, and A. Vidal-Puig. 2011. Origins of metabolic complications in obesity: ectopic fat accumulation. The importance of the qualitative aspect of lipotoxicity. *Curr. Opin. Clin. Nutr. Metab. Care.* **14:** 520–526.

38. Schultze, J. L., A. Schmieder, and S. Goerdt. 2015. Macrophage activation in human diseases. *Semin. Immunol.* **27:** 249–256.

39. Klöting, N., and M. Blüher. 2014. Adipocyte dysfunction, inflammation and metabolic syndrome. *Rev. Endocr. Metab. Disord.* **15:** 277–287.

40. Giordano, A., A. Frontini, and S. Cinti. 2016. Convertible visceral fat as a therapeutic target to curb obesity. *Nat. Rev. Drug Discov.* **15:** 405–424.

41. Cancello, R., M. C. Zingaretti, R. Sarzani, D. Ricquier, and S. Cinti. 1998. Leptin and UCP1 genes are reciprocally regulated in brown adipose tissue. *Endocrinology.* **139:** 4747–4750.

42. Razzoli, M., A. Frontini, A. Gurney, E. Mondini, C. Cubuk, L. S. Katz, C. Cero, P. J. Bolan, J. Dopazo, A. Vidal-Puig, et al. 2015. Stress-induced activation of brown adipose tissue prevents obesity in conditions of low adaptive thermogenesis. *Mol. Metab.* **5:** 19–33.

43. Cinti, S. 2009. Transdifferentiation properties of adipocytes in the adipose organ. *Am. J. Physiol. Endocrinol. Metab.* **297:** E977–E986.

44. Giordano, A., A. Smorlesi, A. Frontini, G. Barbatelli, and S. Cinti. 2014. White, brown and pink adipocytes: the extraordinary plasticity of the adipose organ. *Eur. J. Endocrinol.* **170:** R159–R171.

45. Lowell, B. B., V. S-Susulic, A. Hamann, J. A. Lawitts, J. Himms-Hagen, B. B. Boyer, L. P. Kozak, and J. S. Flier. 1993. Development of obesity in transgenic mice after genetic ablation of brown adipose tissue. *Nature.* **366:** 740–742.

46. Kopecky, J., G. Clarke, S. Enerback, B. Spiegelman, and L. P. Kozak. 1995. Expression of the mitochondrial uncoupling protein gene from the aP2 gene promoter prevents genetic obesity. *J. Clin. Invest.* **96:** 2914–2923.

47. Roberts-Toler, C., B. T. O'Neill, and A. M. Cypess. 2015. Diet-induced obesity causes insulin resistance in mouse brown adipose tissue. *Obesity (Silver Spring).* **23:** 1765–1770.

48. Yang, X., S. Enerbäck, and U. Smith. 2003. Reduced expression of FOXC2 and brown adipogenic genes in human subjects with insulin resistance. *Obes. Res.* **11:** 1182–1191.

49. Cypess, A. M., S. Lehman, G. Williams, I. Tal, D. Rodman, A. B. Goldfine, F. C. Kuo, E. L. Palmer, Y. H. Tseng, A. Doria, et al. 2009. Identification and importance of brown adipose tissue in adult humans. *N. Engl. J. Med.* **360:** 1509–1517.

50. Dinh, C. H., A. Szabo, Y. Yu, D. Camer, Q. Zhang, H. Wang, and X. F. Huang. 2015. Bardoxolone methyl prevents fat deposition and inflammation in brown adipose tissue and enhances sympathetic activity in mice fed a high-fat diet. *Nutrients.* **7:** 4705–4723.

51. Polyák, A., Z. Winkler, D. Kuti, S. Ferenczi, and K. J. Kovács. 2016. Brown adipose tissue in obesity: Fractalkine-receptor dependent immune cell recruitment affects metabolic-related gene expression. *Biochim. Biophys. Acta.* **1861:** 1614–1622.

52. Sakamoto, T., T. Nitta, K. Maruno, Y. S. Yeh, H. Kuwata, K. Tomita, T. Goto, N. Takahashi, and T. Kawada. 2016. Macrophage infiltration into obese adipose tissues suppresses the induction of UCP1 level in mice. *Am. J. Physiol. Endocrinol. Metab.* **310:** E676–E687.

53. Schreiber, R., C. Diwoky, G. Schoiswohl, U. Feiler, N. Wongsiriroj, M. Abdellatif, D. Kolb, J. Hoeks, E. E. Kershaw, S. Sedej, et al. 2017. Cold-induced thermogenesis depends on ATGL-mediated lipolysis in cardiac muscle, but not brown adipose tissue. *Cell Metab.* **26:** 753–763.e7.

54. Haemmerle, G., T. Moustafa, G. Woelkart, S. Büttner, A. Schmidt, T. van de Weijer, M. Hesselink, D. Jaeger, P. C. Kienesberger, K. Zierler, et al. 2011. ATGL-mediated fat catabolism regulates cardiac mitochondrial function via PPAR-α and PGC-1. *Nat. Med.* **17:** 1076–1085.

55. Müller, T. D., S. J. Lee, M. Jastroch, D. Kabra, K. Stemmer, M. Aichler, B. Abplanalp, G. Ananthakrishnan, N. Bhardwaj, S. Collins, et al. 2013. P62 links β-adrenergic input to mitochondrial function and thermogenesis. *J. Clin. Invest.* **123:** 469–478.

56. Shimizu, I., T. Aprahamian, R. Kikuchi, A. Shimizu, K. N. Papanicolaou, S. MacLauchlan, S. Maruyama, and K. Walsh. 2014. Vascular rarefaction mediates whitening of brown fat in obesity. *J. Clin. Invest.* **124:** 2099–2112.

57. Legrand-Poels, S., N. Esser, L. L'Homme, A. Scheen, N. Paquot, and J. Piette. 2014. Free fatty acids as modulators of the NLRP3 inflammasome in obesity/type 2 diabetes. *Biochem. Pharmacol.* **92:** 131–141.

58. van Marken Lichtenbelt, W. D., J. W. Vanhommering, N. M. Smulders, J. M. Drossaerts, G. J. Kemerink, N. D. Bouvy, P. Schrauwen, and G. J. Teule. 2009. Cold-activated brown adipose tissue in healthy men. *N. Engl. J. Med.* **360:** 1500–1508.

59. Virtanen, K. A., M. E. Lidell, J. Orava, M. Heglind, R. Westergren, T. Niemi, M. Taittonen, J. Laine, N. J. Savisto, S. Enerback, et al. 2009. Functional brown adipose tissue in healthy adults. *N. Engl. J. Med.* **360:** 1518–1525.